Advanced Powder Technology xxx (xxxx) xxx

Contents lists available at ScienceDirect

Advanced Powder Technology

journal homepage: www.elsevier.com/locate/apt

Original Research Paper

Impact of grinding media on high-energy ball milling-driven amorphization in multiparticulate $As_4S_4/ZnS/Fe_3O_4$ nanocomposites

Oleh Shpotyuk [a,b,*], Zdenka Lukáčová Bujňáková [c], Peter Baláž [c], Yaroslav Shpotyuk [d,e], Pavlo Demchenko [f], Valentina Balitska [g]

[a] Faculty of Mathematics and Natural Sciences, Jan Dlugosz University in Czestochowa, 13/15, al. Armii Krajowej, Czestochowa 42200, Poland
[b] Department of Optical Glass and Ceramics, O.G. Vlokh Institute of Physical Optics, 23, Dragomanova st., Lviv 79005, Ukraine
[c] Department of Mechanochemistry, Institute of Geotechnics of Slovak Academy of Sciences, 45, Watsonova str., Košice 04001, Slovakia
[d] Department of Sensor and Semiconductor Electronics, Ivan Franko National University of Lviv, 107, Tarnavskoho st., Lviv 79017, Ukraine
[e] Institute of Physics, University of Rzeszow, 1, Pigonia st., 35959 Rzeszow, Poland
[f] Department of Inorganic Chemistry, Ivan Franko National University of Lviv,6-8, Kyryla i Myfodia st., Lviv 79005, Ukraine
[g] Department of Physics and Chemistry of Burning, Lviv State University of Life Safety, 35, Kleparivska str., Lviv 79007, Ukraine

ARTICLE INFO

Article history:
Received 28 March 2020
Received in revised form 24 June 2020
Accepted 8 July 2020
Available online xxxx

Keywords:
Powder technology
Mechanical milling
Amorphization
Arsenic sulphide β-As_4S_4

ABSTRACT

Amorphization scenarios in multiparticulate grinding media composed of $As_4S_4/ZnS/Fe_3O_4$ nanocomposites driven by high-energy ball mechanical milling are identified employing the X-ray powder diffraction analysis on intermediate-range ordering in the generated amorphous phase. This amorphous phase is supposed to be nucleated heterogeneously from grain boundaries of β-As_4S_4 crystallites followed by penetration deeply into grain interior, stabilizing the crystalline-amorphous core-shell structure of the fine-grained nanoparticles. Coexistence of nanocrystalline nc-β-As_4S_4 and amorphous arsenic monosulphide a-AsS phases is crucial feature of these nanocomposites, the amorphous substance being generated continuously due to *re-amorphization* of disordered phase initially existed in arsenic sulphide prepared by synthesis from elements and direct milling-driven vitrification of nc-β-As_4S_4. In monoparticulate β-As_4S_4-based and biparticulate As_4S_4/Fe_3O_4 nanocomposites, the amorphizing configurations are composed of single- and triple-broken chain-like network clusters. Under stronger conditions realized in the grinding medium composed by hard nanoparticles biased by their sizes in respect to 20:1 rule, as in triparticulate $1{\cdot}As_4S_4$-4·ZnS-$1{\cdot}Fe_3O_4$ nanocomposite, the amorphization scenario differs being activated by double-breaking of intramolecular covalent bonds within As_4S_4 cage-like molecules. This effect is identified as nanocrystalline nc-ZnS-assisted milling-driven arsenic monosulphide amorphization in triparticulate $1{\cdot}\beta$-As_4S_4-4·ZnS-$1{\cdot}Fe_3O_4$ nanocomposite solution.

1. Introduction

The high-energy mechanical milling (MM), also termed as *nanomilling*, is one of the fastest growing and widespread materials-processing technologies in the engineering of advanced *nanostructured materials* with functionalizing length-scale below ~100 nm, which possess variety of properties important for implementation in different spheres of human activity [1–3]. In substances with developed predisposition to high-entropy state, the MM-induced *nanostructurization* is often accompanied with *amorphization*, the process of disordering owing to generation of structural defects and mechanical strain under multiple interparticle collisions, tension, crushing [4–7]. The high-temperature modification of tetra-arsenic tetra-sulphide polymorph β-As_4S_4 (viz. the arsenic monosulphide) possessing promising anticancer (antitumor) activity [8,9] belongs to a great family of such *amorphizing-prone* biomedical materials [10,11]. Indeed, if this compound is prepared from elements by direct synthesis, it always shows an accompanied amorphous phase [10]. Balance between *native* crystalline and amorphous phases can be disturbed under nanomilling, following diversity in the amorphization scenarios activated in respect to the Gibbs free energy gained in the amorphizing system [12–15].

In case of *multi-nanoparticulate substances*, the nanostructurization-amorphization relations are essentially

* Corresponding author at: Faculty of Mathematics and Natural Sciences, Jan Dlugosz University in Czestochowa, 13/15, al. Armii Krajowej, Czestochowa 42200, Poland.
E-mail address: o.shpotyuk@ujd.edu.pl (O. Shpotyuk).

https://doi.org/10.1016/j.apt.2020.07.008
0921-8831/

governed by type of grinding media, controlling both energy transfer from milling tools to amorphizing powder, as well as energy re-transfer between milling nanoparticles [16–18]. Thus, e.g., the salt (NaCl or KCl) was used recently as solid solvent in heterogeneous solution to assist the MM synthesis of some pre-grind hierarchically porous metal-organic frameworks [19]. In our preliminary research [12–15], this *nanostructurization-amorphization balance* was specified for *monoparticulate* medium based exceptionally on β-As_4S_4 nanocrystallites [12,13], *biparticulate* (As_4S_4/Fe_3O_4) medium composed of comparable amount of equally-sized β-As_4S_4 and magnetite Fe_3O_4 crystallites [14], and *triparticulate* (As_4S_4/ZnS/Fe_3O_4) medium additionally enriched in zinc sulphide ZnS nanoparticles [15] activated under high-energy MM at different rotational speeds. In all these multi-particulate grinding media, the amorphous phase continuously generated under speed-increased MM (in full respect to "shell" kinetic model [4,7]) was probably of the same chemistry (originated from arsenic sulphide), nevertheless, more strict pre-conditions of its appearance was rather unclear in view of deviation in the milling parameters.

The objective of the current research is to compare amorphization scenarios in monoparticulate, biparticulate and triparticulate β-As_4S_4-based grinding media of (As_4S_4/ZnS/Fe_3O_4) type activated under the same high-energy ball MM conditions, employing the X-ray powder diffraction (XRPD) studies on medium-range structural ordering in the generated amorphous phase.

2. Materials and methods

2.1. Multiparticulate β-As_4S_4-based grinding media and dry-milling technology

Commercial high-temperature arsenic sulphide β-As_4S_4 polymorph of 95% purity purchased in Sigma-Aldrich (USA) and natural mineral magnetite Fe_3O_4 obtained from the mine Kiruna (Sweden) were used as starting materials in the grinding media preparation, while zinc acetate and sodium sulphide were used as precursors for zinc sulphide ZnS preparation through chemical reactions.

To prepare *monoparticulate* grinding media, small pieces of commercial arsenic monosulphide were coarse-grained, powdered and sieved under 200 μm. Then, this powder (in a total amount of 3 g) was subjected to MM in a dry mode under protective Ar atmosphere, using the planetary ball mill Pulverisette 6 (Fritsch, Germany). This procedure was performed in 250 mL WC milling chamber with 50 WC milling balls (each having 10 mm in diameter) under stabilized rotational speed of the planet carrier approaching n = 500 min^{-1}, the overall milling duration being 20 min.

The *biparticulate* 4·As_4S_4-1·Fe_3O_4 and 1·As_4S_4-1·Fe_3O_4 grinding media were prepared under the same MM conditions, using coarse-grained arsenic monosulphide and mineral magnetite Fe_3O_4 in the molar proportions of 4:1 and 1:1.

To prepare *triparticulate* grinding media based on 1·As_4S_4-4·ZnS-1·Fe_3O_4 nanocomposite, the ZnS precursors (zinc acetate $(CH_3COO)_2Zn{\cdot}2H_2O$, 99%, Ites; and sodium sulphide $Na_2S{\cdot}9H_2O$, 98%, Acros Organics) were co-milled under the same milling conditions according to the following equation:

$$As_4S_4 + 4{\cdot}(CH_3COO)_2Zn{\cdot}2{\cdot}H_2O + 4{\cdot}Na_2S{\cdot}9H_2O + Fe_3O_4 \rightarrow$$

$$\rightarrow 1{\cdot}As_4S_4/4{\cdot}ZnS/1{\cdot}Fe_3O_4 + 8{\cdot}(CH_3COO)Na + 44H_2O \quad (1)$$

After reaction (1), the resultant sodium acetate was removed from the product by washing with distilled water and drying (70 °C, 180 min) to separate solid phase remainder, which roughly keeps 1:4:1 ratio between molar fractions of components (β-As_4S_4, ZnS, Fe_3O_4).

In all the above cases of multi-particulate grinding media, the energy transfers from the mill to fine-grained powdered system estimated over specific grinding work performed in the planetary ball mill Pulverisette 6 [16–18] was estimated to approach ~105 kJ/g.

2.2. Nanocrystalline structure identification

Crystallographic specificity of the studied (As_4S_4/ZnS/Fe_3O_4) nanocomposites was identified with the XRPD analysis in transmission mode employing the STOE STADI P diffractometer (STOE & Cie GmbH, Darmstadt, Germany) with linear position-sensitive detector (Cu Kα_1 radiation, curved Ge(1 1 1) monochromator), as was specified in more details elsewhere [13–15]. The microstructure of crystallites (average apparent crystallite size D, average maximum strain ε) of arsenic monosulphide β-As_4S_4 (JCPDS card No. 72-0686) [11,20], magnetite Fe_3O_4 (JCPDS card No. 74-0748) [21], low-temperature cubic ZnS (sphalerite, JCPDS card No. 05-0566) and high-temperature hexagonal ZnS (wurtzite, JCPDS card No. 70-2204) [22] were defined by the Rietveld refinement method using the FullProf.2 k (v.5.40) program [23] in terms of isotropic line broadening [24], applying a pseudo-Voigt profile function and isotropic approximation for the atomic displacement parameters. The calibration procedure was performed utilizing SRM 640b (Si) [25] and SRM 676 (Al_2O_3) [26] NIST standards.

2.3. Amorphous phase characterization

The amorphous phase appeared under high-energy MM in chalcogenide network-forming substances like As-S can be clarified with XRPD analysis applied to their diffuse "amorphous" halos positioned near ~15–22 °2θ, ~28–36 °2θ and ~50–60 °2θ [27–29]. According to Fourier-transform analysis [23], each of these halos corresponds to some kinds of real-space ordering in network glass-formers. Thus, the first of these halos at ~15–22 °2θ (i.e. at scattering vectors Q approaching ~1.2–1.3 $Å^{-1}$) reproduced in the structure factor as first sharp diffraction peak (FSDP) is associated with length scale commensurable with *intermediate-range ordering* of glass-forming species [28]. For glassy networks composed of directional covalent-bonded units, the next halo at ~28–36 °2θ (viz. Q ~ 2.2–2.3 $Å^{-1}$) referred to as the principal diffraction peak (PDP) in terms of [28], or second sharp diffraction peak (SSDP) in the Elliott's terminology [30], is ascribed to *size of local network-forming motifs*, which are deterministic for so-called *extended-range ordering* in amorphous structure [31,32]. At last, the halo observed at ~50–60 °2θ (viz. Q ~ 3.3–4.0 $Å^{-1}$) concerns *nearest-neighbor separations* between constituting atoms [28].

The halos structure of the MM-driven amorphizing phase was identified from experimental XRPD patterns processed with STOE WinXPOW 3.03 [33] and PowderCell 2.4 [34] program packages following normalization in respect to the intensity of the maximum peak. These data were used for next profile fitting with WinPLOTR program [33]. Both *peak angular position* (2θ) and *full width at half maximum* (FWHM) were defined with ±0.05 °2θ accuracy, the respective values of *scattering vector* Q and *width* ΔQ in a reciprocal space being calculated as:

$$Q = (4\pi/\lambda)\cdot\sin\theta, \quad (2)$$

$$\Delta Q = (4\pi/\lambda)\cdot\sin(FWHM/2) \quad (3)$$

The *characteristic distance* R (spacing of peak-responsible quasi-periodicity) and *correlation length* L over which this quasi-periodicity is maintained was defined as [28,29]:

$$R = 2\pi/Q, \quad (4)$$

Please cite this article as: O. Shpotyuk, Z. L. Bujňáková, P. Baláž et al., Impact of grinding media on high-energy ball milling-driven amorphization in multiparticulate As_4S_4/ZnS/Fe_3O_4 nanocomposites, Advanced Powder Technology, https://doi.org/10.1016/j.apt.2020.07.008

$$L = 2\pi/\Delta Q. \quad (5)$$

In our interpretation, we also explore the concept of diffuse halos in the XRPD patterns of amorphous substances, treated them as arising from coordination spheres, i.e. the closest inter-atomic distances like in randomly-packed multiparticulate systems [35–38], when XRPD patterns are governed by the known Ehrenfest relation [39]:

$$2ds \cdot \sin\theta = 1.23 \cdot \lambda \quad (6)$$

where d_s is an average *inter-atomic distance* in a glass structure (i.e. distance between scattering centers defined as radius of the corresponding coordination sphere).

Thus, the intermediate-range ordering in the MM-derived amorphous phase was specified with XRPD analysis applied to the FSDP, which is indicative of structural entities over a scale of a few tens of Å [30,31]. A straightforward interpretation of this phenomenon is developed at the basis of *modified microcrystalline approach* [40–42] treating this halo as a superposition of broadened Bragg-diffraction reflexes from some remnants of crystalline *inter-planar correlations R*, supplemented by reflexes from most prominent *pair inter-atomic correlations* d_s, i.e. diffuse halos from coordination spheres obeying the Ehrenfest relation (6). The latter is known to be useful approach for *ideal amorphous solids*, characterized by structures composed of randomly-positioned hard spheres obeying dense random packing arrangement [35–38].

3. Results and discussion

Experimental XRPD patterns of monoparticulate, biparticulate and triparticulate β-As_4S_4-based grinding media activated by high-energy ball MM under abovementioned conditions are depicted on Figs. 1 and 2.

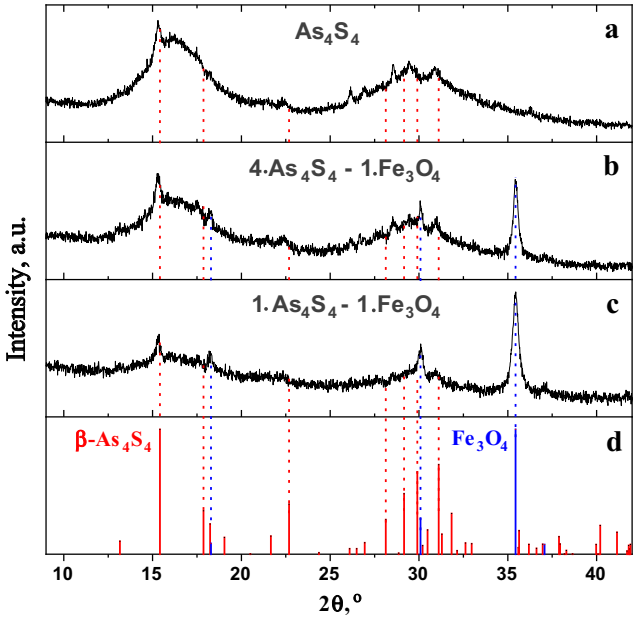

Fig. 1. Observed XRPD profile of fine-grained powdered nanocomposites MM-activated from arsenic monosulphide As_4S_4 (a), 4·As_4S_4-1·Fe_3O_4 (b), and 1·As_4S_4-1·Fe_3O_4 grinding media (c), as compared with calculated Bragg-diffraction reflexes from constituent crystalline phases (d), the high-temperature β-As_4S_4 (red-colored, JCPDS card No. 72–0686) and magnetite Fe_3O_4 (blue-colored, JCPDS card No. 74–0748). (For interpretation of the references to colour in this figure legend, the reader is referred to the web version of this article.)

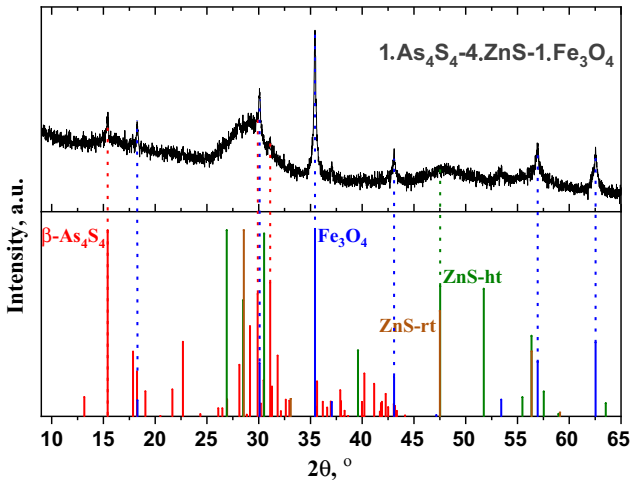

Fig. 2. Observed XRPD profile of 1·β-As_4S_4-4·ZnS-1·Fe_3O_4 nanocomposite (black solid line at the top) compared with calculated Bragg diffraction reflexes from constituent phases (at the bottom) of β-As_4S_4 (red-colored, JCPDS card No. 72-0686), magnetite Fe_3O_4 (blue-colored, JCPDS card No. 74-0748), high-temperature ZnS wurtzite (green-colored, JCPDS card No. 79-2204) and room-temperature ZnS sphalerite (brown-colored, JCPDS card No. 05-0566). (For interpretation of the references to colour in this figure legend, the reader is referred to the web version of this article.)

3.1. Monoparticulate β-As_4S_4-based grinding medium

The β-As_4S_4 crystalline phase [11,20] prevails in the XRPD pattern of this monoparticulate grinding medium (see Fig. 1a) with intensive Bragg-diffraction reflections, corresponding to interplanar distances of $d(\bar{1}11)$ = 5.745 Å (15.41°2θ, I = 100%), $d(\bar{2}\ 2\ 2)$ = 2.873 Å (31.11°2θ, I = 71.7%), $d(221)$ = 2.986 Å (29.90°2θ, I = 65.8%), $d(311)$ = 3.060 Å (29.16°2θ, I = 48.4%) and $d(\bar{1}12)$ = 3.917 Å (22.68°2θ, I = 40.0%). These reflections are essentially broadened in a width and slightly shifted towards lower diffraction angles 2θ corresponding to prolonged inter-planar distances and, respectively, reduced densities of MM-driven nanocrystalline phase (nc-β-As_4S_4), like its character for vapor-deposited amorphous Si films is affected to crystallization annealing [43]. The calculated average apparent crystallite size D is close to ~20 nm and average maximum strain ε approaches 0.0070 [44,45]. Measurement of specific surface area S_{BET} = 0.47 m^2g^{-1} for nc-β-As_4S_4 confirms strong interaction between crystallites resulted in aggregation and agglomeration, with polymodal particle size distribution profile in a submicron range with a few maxima at ~300, ~550 and ~850 nm [44]. Decaying background and broad diffuse halos on the XRPD profiles near ~16°2θ, 32°2θ and 56°2θ (see Fig. 1a) correspond to accompanied amorphous a-AsS phase generated under high-energy MM in protective Ar atmosphere in respect to reaction:

$$\beta - As_4S_4 \xrightarrow{\text{dry-MMinAr}} nc - \beta - As_4S_4 + a - AsS \quad (7)$$

Detailed inspection of the XRPD profile on Fig. 1 after subtracting reflexes ascribed to nc-β-As_4S_4, allows refinement of the FSDP (see Fig. 3a) attributed to intermediate-range ordering in the MM-derived amorphous phase, the corresponding parameters being gathered in Table 1.

The FSDP being very narrowed in a reciprocal space due to small ΔQ = 0.31 $Å^{-1}$ is positioned near scattering vector Q = 1.15 $Å^{-1}$ (Table 1). These parameters are in monotonic dependence with those character for upgoing sequence of melt-quenched $As_{40}S_{60}$ glass [40,46], $As_{42}S_{58}$ glass [46], and MM-amorphized $As_{45}S_{55}$ alloy [47]. Within modified microcrystalline approach [40–42], the FSDP of compositionally authentic amorphous phase MM-derived from

Please cite this article as: O. Shpotyuk, Z. L. Bujňáková, P. Baláž et al., Impact of grinding media on high-energy ball milling-driven amorphization in multiparticulate As_4S_4/ZnS/Fe_3O_4 nanocomposites, Advanced Powder Technology, https://doi.org/10.1016/j.apt.2020.07.008

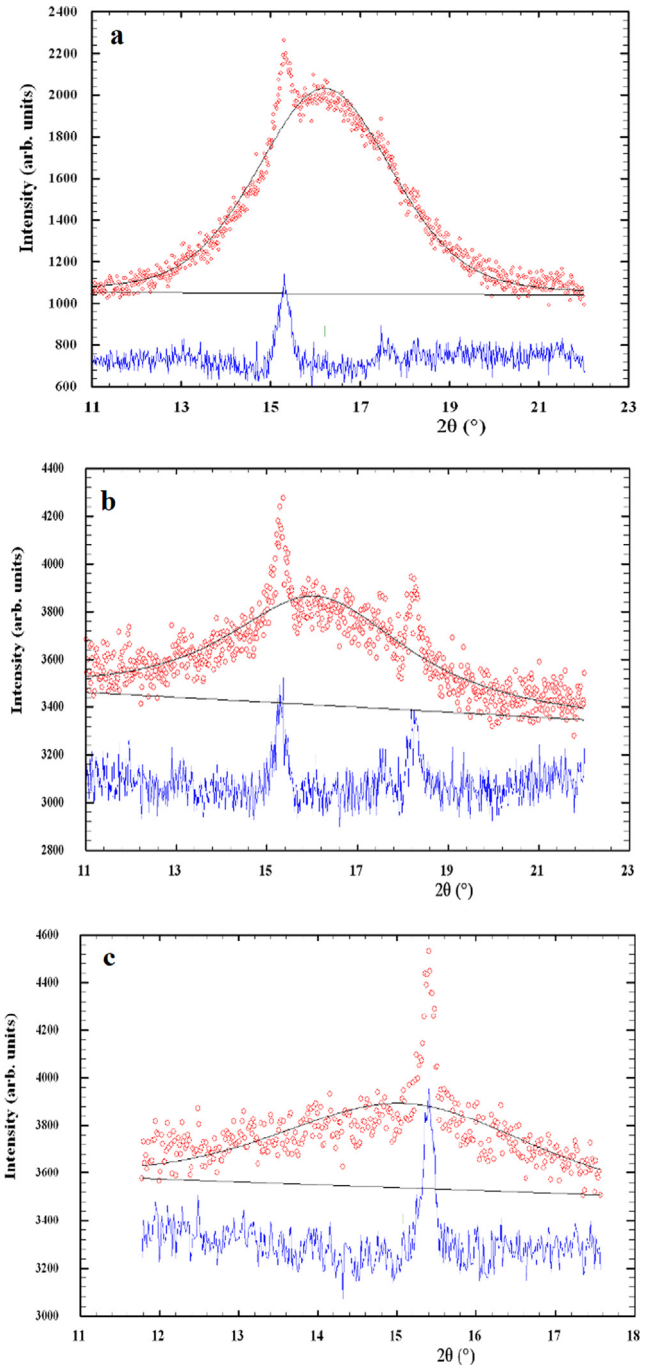

Fig. 3. Experimental (red-pointed) and calculated (black solid line) XRPD patterns showing profile fitting of the FSDP (the difference is given at the bottom by blue solid curve) for amorphous phase MM-derived from monoparticulate arsenic monosulphide As_4S_4 (a), biparticulate $1{\cdot}As_4S_4$-$1{\cdot}Fe_3O_4$ (b), and triparticulate $1{\cdot}As_4S_4$-$4{\cdot}ZnS$-$1{\cdot}Fe_3O_4$ grinding media (c). (For interpretation of the references to colour in this figure legend, the reader is referred to the web version of this article.)

β-As_4S_4 grinding media can be reasonably understood as originated from inter-planar correlations of some remnants of crystalline structures (having R = 5.46 Å and L = 24.7 Å) superimposed by prominent inter-atomic correlations around d_s = 6.72 Å. Assuming the FSDP position in the amorphized AsS as averaged superposition of most prominent inter-planar correlations related to molecular-type structure of β-As_4S_4 with $d(\bar{1}11)$ = 5.75 Å and layer-type structure of orpiment As_2S_3 with $d(020)$ = 4.79 Å, the density of this MM-derived amorphous phase is estimated to be ~3.43 g·cm^{-3} [15].

Thus, the MM-driven amorphization in arsenic monosulphide can be imagined as transition from molecular structure proper for β-As_4S_4 to structural arrangement of network derivatives originated from these As_4S_4 molecules, which appear due to breaking of some intra-molecular bonds and forming inter-molecular ones instead. The most plausible topological configurations of such networks were recognized at the basis of smallest cluster-forming energies calculated with *ab-initio* quantum-chemical modeling code CINCA [13,15], these being composed by optimally-constrained single x1-broken atomic clusters keeping one hexagon and two pentagons and over-constrained completely polymerized triple x3-broken clusters in chain-like configuration (Fig. 4).

The energetic specificity of molecular-to-network transitions in arsenic monosulphide can be reflected in the developed combined configuration-enthalpy landscape [48], which evolves configuration-coordinate presentation of the cluster-forming energies E_f and respective barriers of molecular-to-network transitions ΔE_f superimposed with enthalpy diagram of structural relaxation in the amorphizing system (see Fig. 5). Specifically, the MM-driven amorphization in monoparticulate β-As_4S_4-based grinding medium occurs from two different sources, these being (i) re-amorphization of amorphous phase initially existed in the arsenic monosulphide synthesized from elemental ingredients and (ii) direct vitrification of nc-β-As_4S_4 with $\Delta E_f \sim 0.71$ kcal/mol for x1-broken atomic clusters and $\Delta E_f \sim 1.14$ kcal/mol for x3-broken clusters (scenario 2 on Fig. 4). Our recent data [45] testify in a favor of "shell" kinetic model describing this process due to generation of structural defects in the nc-β-As_4S_4, the isocompositional amorphous phase being nucleated heterogeneously starting from grain boundaries and followed by penetration deeply into grain interior (as illustrated for nanoparticle constitution shown in Fig. 6a). So under high-energy MM-activation of β-As_4S_4 medium, the fine-grained arsenic monosulphide nanoparticles (probably of crystalline-amorphous core-shell structure) are stabilized in the resultant fine-grained powder substance.

3.2. Biparticulate (As_4S_4/Fe_3O_4) grinding media

Under the same milling conditions, the similar amorphization pathways can be activated for other fine-grained nanopowders MM-derived from biparticulate grinding medium composed of arsenic monosulphide with addition of mineral magnetite Fe_3O_4 [14,15], the XRPD patterns for $4{\cdot}As_4S_4$-$1{\cdot}Fe_3O_4$ and $1{\cdot}As_4S_4$-$1{\cdot}Fe_3O_4$ grinding media are shown in Fig. 1b and 1c, respectively. These nanopowders contain both types of crystallites, the nc-β-As_4S_4 [11,20] and nc-Fe_3O_4 [21].

The latter contributes to the XRPD patterns through broadened Bragg-diffraction reflexes corresponding to interplanar distances of $d(220)$ = 2.968 Å (30.09°2θ, I = 28.5%), $d(311)$ = 2.531 Å (35.44°2θ, I = 100%), $d(400)$ = 2.099 Å (43.07°2θ, I = 21.2%), $d(333)$ = 1.615 Å (56.96°2θ, I = 29.5%) and $d(440)$ = 1.484 Å (62.55°2θ, I = 40.0%) in the cubic $Fd\bar{3}m$ structure of magnetite Fe_3O_4 with unit cell parameter approaching 8.3941 Å. There are no detectable changes in angular positions of these peaks respectively to theoretical ones (Fig. 1), testifying that the MM-driven nanostructurization of nc-Fe_3O_4 phase is not accompanied by amorphization. The estimated value of average crystallite size D of nc-Fe_3O_4 is ~21 nm for $4{\cdot}As_4S_4$-$1{\cdot}Fe_3O_4$ and ~16 nm for $1{\cdot}As_4S_4$-$1{\cdot}Fe_3O_4$ grinding media.

The former (the nc-β-As_4S_4) contributes to the XRPD patterns of these grinding media through broadened and shifted Bragg-diffraction reflections, attributed to monoclinic structure of β-As_4S_4. Since these reflections (shifted towards prolonged inter-planar distances d) are superimposed with halos from simultaneously generated amorphous phase, it is difficult to estimate their strict size. Nevertheless, we suppose at the basis of comparison

Please cite this article as: O. Shpotyuk, Z. L. Bujňáková, P. Baláž et al., Impact of grinding media on high-energy ball milling-driven amorphization in multiparticulate As_4S_4/ZnS/Fe_3O_4 nanocomposites, Advanced Powder Technology, https://doi.org/10.1016/j.apt.2020.07.008

Table 1
FSDP parameterization of amorphous arsenic monosulphides MM-derived from β-As_4S_4-based grinding media under 20 min high-energy dry ball MM at n = 500 min^{-1}.

Grinding media	2Θ °	FWHM °	Q $Å^{-1}$	ΔQ $Å^{-1}$	R Å	L Å	d_s Å
Non-milled β-As_4S_4	16.712(13)	4.35(3)	1.185	0.31	5.30	20.3	6.52
Monoparticulate β-As_4S_4	16.213(7)	3.57(2)	1.150	0.25	5.46	24.7	6.72
Biparticulate 4·β-As_4S_4-1·Fe_3O_4	16.197(12)	3.93(4)	1.150	0.28	5.47	22.5	6.73
Biparticulate 1·β-As_4S_4-1·Fe_3O_4	16.068(28)	4.64(11)	1.140	0.33	5.51	19.0	6.78
Triparticulate 1·β-As_4S_4-4·ZnS-1·Fe_3O_4	15.077(3)	3.65(9)	1.070	0.26	5.87	24.2	7.22

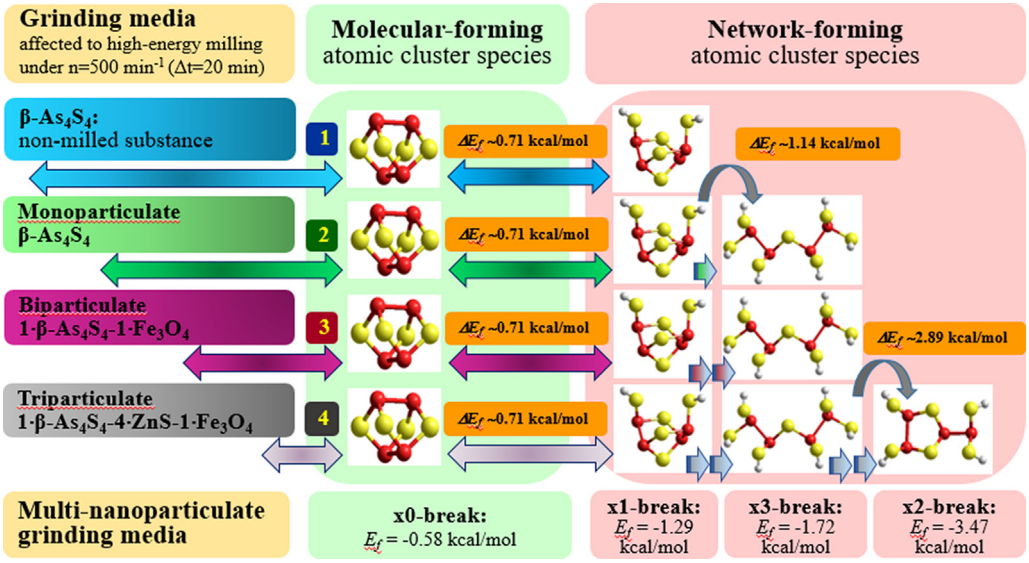

Fig. 4. Amorphization scenarios activated by high-energy MM in multi-nanoparticulate β-As_4S_4-based grinding media. The bottom scale gives molecular and network cluster-forming energies calculated with CINCA modeling code. The colored arrows indicate MM-driven transition to the most plausible network-forming atomic configurations, the energetic barriers of respective molecular-to-network transitions ΔE_f being denoted above arrows (see text for more details).

with the XRPD pattern of MM-activated monoparticulate As_4S_4 (Fig. 1a), the corresponding crystallite size D being rather close to ~20 nm.

With increase in nc-Fe_3O_4 content in biparticulate (As_4S_4/Fe_3O_4) grinding media, the FSDP position Q shifts towards 1.14 $Å^{-1}$ and saturates in width to $\Delta Q \sim 0.33$ $Å^{-1}$ (Fig. 3b), these changes being concomitant with growing trend in the characteristic distance to $R \sim 5.51$ Å and decaying tendency in the correlation length to $L \sim 19.0$ Å (see Table 1). Remarkably, the amorphous phase stabilized under high-energy MM in this solution (1·As_4S_4-1·Fe_3O_4) is very similar to that derived from monoparticulate β-As_4S_4, as it follows from nearly the same saturated position of the FSDP, but shorter correlation length L, which is ascribed to the appeared amorphous phase neighboring with nc-Fe_3O_4 particles.

Therefore, in respect to constitution of this biparticulate (As_4S_4/Fe_3O_4) grinding media shown in Fig. 6b, it seems reasonable assuming that hard nc-Fe_3O_4 nanoparticles (possessing Mohs hardness of 5.5–6.5 [49]) are uniformly distributed among soft nc-β-As_4S_4 nanoparticles of almost the same sizes covered by amorphous a-AsS phase (having, at least, three-times less hardness [49]). With increased nc-Fe_3O_4 content, the MM-gained free energy is more effectively transferred to nc-β-As_4S_4, ensuring quicker saturation of respective amorphization scenarios connected with network-forming clusters originated from x1-broken and x3-broken cage-like As_4S_4 molecules (depicted by scenario 3 on Fig. 4). Noteworthy, this portion of the MM-transferred energy is insufficient for over-barrier molecular-to-network transition initiated by double x2-broken intramolecular bonds, corresponding to transition in x2-1 state on potential energy landscape with energetic barrier of $\Delta E_f \sim 2.89$ kcal/mol (see Fig. 5).

3.3. Triparticulate 1·As_4S_4-4·ZnS-1·Fe_3O_4 grinding medium

Under stronger ball MM conditions ensuring higher portion of gained energy in the milled substance, the amorphization of arsenic monosulphide cardinally differs being activated by double x2-breaking of intramolecular bonds as shown in the bottom scenario on Fig. 4. This unusual amorphization pathway can be realized in the nc-β-As_4S_4 additionally modified by extra-hard nanoparticles biased by their sizes, as in triparticulate 1·As_4S_4-4·ZnS-1·Fe_3O_4 grinding medium.

The XRPD pattern of 1·As_4S_4-4·ZnS-1·Fe_3O_4 nanocomposite solution activated at the same MM conditions is shown in Fig. 2 as compared with calculated Bragg-diffraction reflexes from all constituent crystalline phases. The nc-Fe_3O_4 phase is revealed due to broadened Bragg-diffraction reflexes ascribed to $Fd\bar{3}m$ structure of magnetite [21]. The apparent crystallite size of coherently diffracting domain for this phase D can be determined from broadening of most intensive $d(311)$ = 2.531 Å line (at 35.44°2θ, I = 100%) resulting in ca. $D \sim 22.4$ nm, while maximum strain is estimated as $\varepsilon \sim 0.0057$. The monoclinic nc-β-As_4S_4 phase [11,20] prevails with Bragg-diffraction lines positioned at 15.41 °2θ, 31.11 °2θ and 29.90 °2θ, corresponding respectively to reflections

Please cite this article as: O. Shpotyuk, Z. L. Bujňáková, P. Baláž et al., Impact of grinding media on high-energy ball milling-driven amorphization in multiparticulate As_4S_4/ZnS/Fe_3O_4 nanocomposites, Advanced Powder Technology, https://doi.org/10.1016/j.apt.2020.07.008

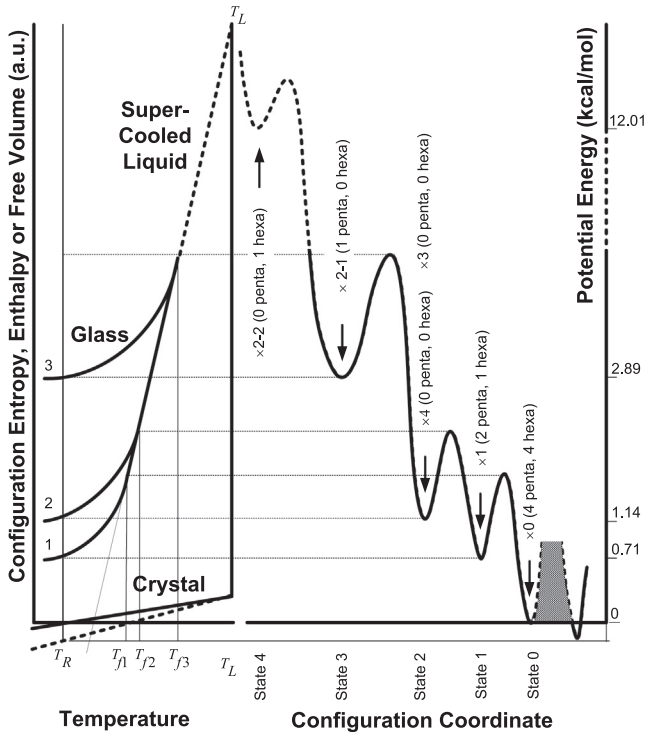

Fig. 5. Combined configuration-enthalpic landscape illustrating MM-driven amorphization scenarios in different multi-nanoparticulate β-As_4S_4-based grinding media. The settle-points corresponding to network clusters derived from As_4S_4 molecules by *x*-fold bond-breaking (keeping some small rings, pentagons and hexagons given in parenthesis) are denoted by arrows with respective cluster-forming energies E_f indicated at the right axis.

from $(\bar{1}11)$, $(\bar{2}22)$, and (221) planes. The apparent crystallite size *D* calculated from broadening of most pronounced 15.41 °2θ line ascribed to $d(\bar{1}11) = 5.745$ Å approaches ca. $D \sim 23.5$ nm (this value is complemented with more than twice higher strain $\varepsilon \sim 0.0121$ as compared with nc-Fe_3O_4).

The both nc-ZnS phases (sphalerite and wurtzite) [22] are also found in this MM-activated 1·As_4S_4-4·ZnS-1·Fe_3O_4 nanocomposite grinding medium. Typically, the average crystallite sizes of nc-ZnS is extracted as estimates from broadened Bragg-diffraction lines at ~29 °2θ (see, e.g., [50]), but this is not a current case in view of overlapping this peak with diffuse halo of a-AsS phase [13]. Therefore, more suitable seems *D* value approaching ca. 1.4 nm estimated for broadened line near ~48 °2θ corresponding to reflections from (220) plane in sphalerite and (110) plane in wurtzite structure [22]. The respective value of maximum strain for this broad peak was found to be substantially increased as compared with other nc phases reaching as high as $\varepsilon = 0.0916$.

The MM-derived amorphous a-AsS phase in this triparticulate grinding solution is manifested in the XRPD pattern via decaying background and diffuse halos at ~15–22 (see Fig. 3c). In contrast to previous cases, this halo corresponding to the FSDP is drastically shifted to lower diffraction angles 2θ (see Table 1), so that it almost completely coincides in angular position with most intensive Bragg-diffraction line corresponding to $d(\bar{1}11) = 5.745$ Å at 15.41 °2θ in the structure of nc-β-As_4S_4 (compare Fig. 3a–c). This halo is also narrowed in a width, testifying that generated amorphous phase in this case is essentially different.

So intermediate-range ordering of MM-derived a-AsS is composed of inter-planar correlations from crystalline remnants with highest characteristic distance $R = 5.87$ Å and correlation length $L = 24.2$ Å, complemented by prominent inter-atomic correlations having $d_s = 7.22$ Å (see Table 1). It means that amount of energy re-transferred to nc-β-As_4S_4 under MM in this grinding solution is substantially enhanced, ensuring stabilization of network-forming clusters originated from double x2-broken As_4S_4 molecules (due to overcoming molecular-to-network barrier $\Delta E_f \sim 2.89$-kcal/mol, Fig. 5), which are slightly over-constrained keeping pentagon-type ring in an atomic arrangement (scenario 4 shown in the bottom part of Fig. 4).

Thus, the finest and most stressed nc-ZnS particles with sizes approaching a few nm act as solid solvents in 1·As_4S_4-4·ZnS-1·Fe_3O_4 grinding solution (see Fig. 6c), providing sufficient energy to be gained from collisions with hard magnetite nc-Fe_3O_4 particles (having $D \sim 22.4$ nm) to amorphizing nc-β-As_4S_4 (with crystallites having $D \sim 23.5$ nm in sizes), thus resulting in disordered network of a-AsS composed by double x2-broken As_4S_4 cage molecules (scenario 4 on Fig. 4).

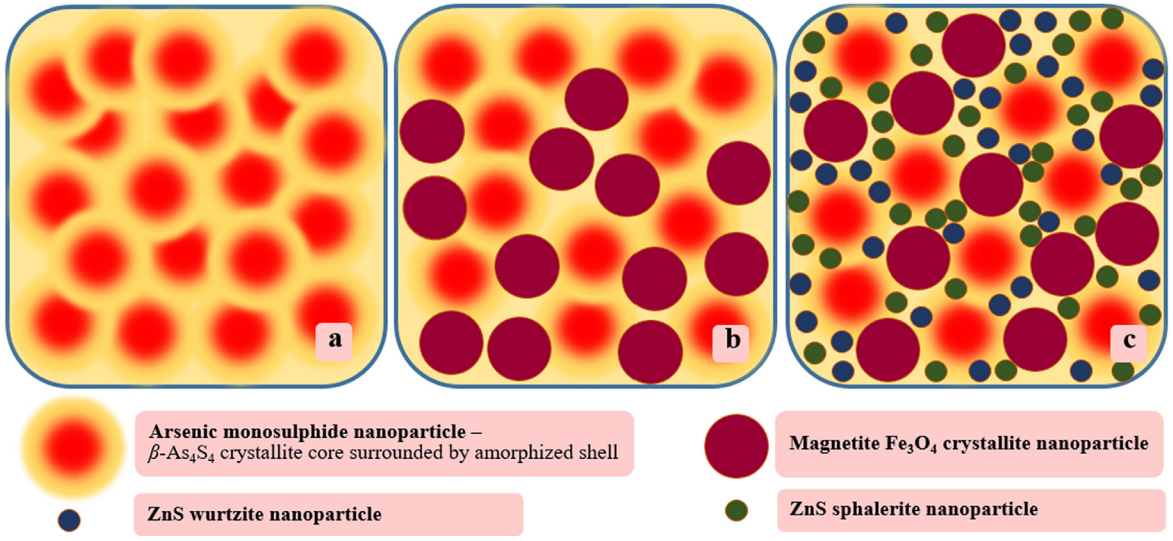

Fig. 6. Schematic drawing showing nanoparticle arrangement in multiparticulate β-As_4S_4-based grinding media: a – monoparticulate As_4S_4, b – biparticulate 1·As_4S_4-1·Fe_3O_4, and c – triparticulate 1·As_4S_4-4·ZnS-1·Fe_3O_4. Arsenic monosulphide nanoparticles composed of β-As_4S_4 crystallite core and isocompositional amorphous shell are red-reddish-toned, magnetite Fe_3O_4 nanoparticles are sharply dark-red-colored, ZnS wurtzite and sphalerite nanoparticles are blue- and green-colored. (For interpretation of the references to colour in this figure legend, the reader is referred to the web version of this article.)

Please cite this article as: O. Shpotyuk, Z. L. Bujňáková, P. Baláž et al., Impact of grinding media on high-energy ball milling-driven amorphization in multiparticulate As_4S_4/ZnS/Fe_3O_4 nanocomposites, Advanced Powder Technology, https://doi.org/10.1016/j.apt.2020.07.008

Under high-energy milling in planetary ball mill, the optimal size of balls ensuring the best breakage of the given size of material is known to be ~20 times as large as the particle size [51]. It seems reasonable to speculate that energy re-transferring between hard nanocrystallites acting as milling balls is also maximized under this ratio between crystallite sizes D, remarkably satisfied in the current case of triparticulate 1·As_4S_4-4·ZnS-1·Fe_3O_4 nanocomposite, biased by particle sizes of amorphizing-prone soft nc-β-As_4S_4 (D ~ 23.5 nm), respectively stable hard nc-ZnS (D ~ 1.4 nm) and extra-hard nc-Fe_3O_4 (D ~ 22.4 nm).

The similar effect was reported recently for NaCl and KCh salts, acting as solid solvents to assist the MM-synthesis of hierarchical porous metal-organic frameworks with high iodine I_2 vapour uptake [19]. The most effective energy re-transfer within such nanocomposite system is achieved due to enhanced hardness of energy re-transferring agents, i.e. nc-ZnS particles, which are essentially reinforced being mediated to nanosize due MM-induced nanostructurization [52,53]. Specifically, in view of this similarity with effect of salt in [19], this phenomenon can be identified as nc-ZnS-assisted MM-driven arsenic monosulphide amorphization (a-AsS) in triparticulate 1·β-As_4S_4-4·ZnS-1·Fe_3O_4 nanocomposite grinding solution.

4. Conclusions

The objective of this research is to compare amorphization scenarios in different β-As_4S_4-based grinding media of (As_4S_4/ZnS/Fe_3O_4) type activated under the same high-energy ball MM conditions, employing the X-ray powder diffraction (XRPD) studies on medium-range structure in the generated amorphous phase. Straightforward interpretation of the results is developed at the basis of modified microcrystalline approach treating first diffuse halo (viz. first sharp diffraction peak, the FSDP) in the XRPD patterns of amorphizing substance as superposition of broadened Bragg-diffraction reflexes originated from remnants of microcrystalline inter-planar correlations, supplemented by the Ehrenfest-diffraction halos from prominent pair inter-atomic correlations.

Coexistence of milling-driven nanocrystalline nc-β-As_4S_4 and amorphous a-AsS phases is crucial feature of these fine-grained nanocomposites. The amorphization in the multi-particulate As_4S_4/ZnS/Fe_3O_4 nanocomposite media occurs from two sources, these being re-amorphization of amorphous phase initially existed in arsenic monosulphide prepared from elements and direct vitrification of nc-β-As_4S_4. The generated amorphous phase is nucleated heterogeneously from nc-β-As_4S_4 grain boundaries followed by penetration deeply into grain interior, so stabilizing the character *crystalline-amorphous core-shell structure* of arsenic monosulphide nanoparticles.

In monoparticulate β-As_4S_4-based and biparticulate (As_4S_4/Fe_3O_4) media, the amorphizing substance is composed of single x1-broken and triple x3-broken chain-like network clusters. Under stronger conditions realized in the grinding solution composed by hard nanoparticles biased by their sizes in respect to 20:1 rule, as in triparticulate 1·As_4S_4-4·ZnS-1·Fe_3O_4 nanocomposite, amorphization scenario cardinally differs being activated by double x2-breaking of intramolecular bonds within As_4S_4 cage-like molecules. This effect is identified as nc-ZnS-assisted MM-driven arsenic monosulphide amorphization in 1·β-As_4S_4-4·ZnS-1·Fe_3O_4 nanocomposite medium.

Declaration of Competing Interest

The authors declare that they have no known competing financial interests or personal relationships that could have appeared to influence the work reported in this paper.

Acknowledgements

This work is supported by the Slovak Research and Development Agency under the contract no. APVV-18-0357, Slovak Grant Agency VEGA (projects 2/0065/18, 2/0044/18). The paper is part of scientific research done within the project No 0119U100357, subject of Scientific Program funded by the Ministry of Education and Science of Ukraine for years 2019-2022.

References

[1] P. Baláž, Mechanochemistry in Nanoscience and Minerals Engineering, Springer, Berlin- Heidelberg, 2008.
[2] P. Baláž, M. Achimovičová, M. Baláž, P. Billik, Z. Cherkezova-Zheleva, J. Manuel Criado, F. Delogu, E. Dutkova, E. Gaffet, F.J. Gotor, R. Kumar, I. Mitov, T. Rojac, M. Senna, A. Streletskii, K. Wieczorek-Ciurowa, Hallmarks of mechanochemistry: from nanoparticles to technology, Chem. Soc. Rev. 42 (2013) 7571–7637, https://doi.org/10.1039/C3CS35468G.
[3] E. Gaffet, G. Le Caer, Mechanical processing for nanomaterials, in: H.S. Nalwa (Ed.), Encyclopedia of Nanoscience and Nanotechnology, American Sci. Publ., vol. X, 2004, pp. 1–39.
[4] R.B. Schwarz, R.R. Petrich, C.K. Saw, The synthesis of amorphous NiTi alloy powders by mechanical alloying, J. Non-Cryst. Solids 76 (1985) 281–302, https://doi.org/10.1016/0022-3093(85)90005-5.
[5] Y.H. Zhao, Z.H. Jin, K. Lu, Mechanical-milling-induced amorphization of Se: a crystallite destabilization model, Phil. Mag. Lett. 79 (1999) 747–754, https://doi.org/10.1080/095008399176814.
[6] L. Piot, S. Le Floch, T. Cornier, S. Daniele, D. Machon, Amorphization in nanoparticles, J. Phys. Chem. C 117 (2011) 11133–11140, https://doi.org/10.1021/jp401121c.
[7] A. Qiao, H. Yang, H.Y. Xiao, J. Xiao, X.P. Liu, Z.R. Ge, R.H. Chen, Milling-induced amorphization in a chalcogenide compound, Chalcogenide Lett. 14 (2017) 195–201. http://www.chalcogen.ro/195_QiaoA.pdf.
[8] P. Baláž, A.V. Nguyen, M. Fabián, D. Cholujová, M. Pastorek, J. Sedlák, Z. Bujňáková, Properties of arsenic sulphide As_4S_4 nanoparticles prepared by high-energy milling, Powder Technol. 211 (2011) 232–236, https://doi.org/10.1016/j.powtec.2011.04.027.
[9] Z. Bujňáková, P. Baláž, P. Makreski, G. Jovanovski, M. Caplovicova, L. Caplovic, O. Shpotyuk, A. Ingram, T.-C. Lee, J.-J. Cheng, J. Sedlak, E. Turianicova, A. Zorkovska, Arsenic sulphide nanoparticles prepared by milling: properties, free-volume characterization, and anti-cancer effects, J. Mater. Sci. 50 (2015) 1973–1985, https://doi.org/10.1007/s10853-014-8763-5.
[10] A. Hrubý, A study of glass-forming ability and phase diagram of the As-S system, J. Non-Cryst. Solids 28 (1978) 139–142, https://doi.org/10.1016/0022-3093(78)90080-7.
[11] P. Bonazzi, L. Bindi, A crystallographic review of arsenic sulphides: effects of chemical variations and changes induced by exposure to light, Z Kristallogr. 223 (2008) 132–147, https://doi.org/10.1524/zkri.2008.0011.
[12] P. Baláž, M. Baláž, O. Shpotyuk, P. Demchenko, M. Vlček, M. Shopska, J. Briančin, Z. Bujňáková, Ya. Shpotyuk, B. Selepová, L. Balážová, Properties of arsenic sulphide (β-As_4S_4) modified by mechanical activation, J. Mater. Sci. 52 (2017) 1747–1758, https://doi.org/10.1007/s10853-016-0466-7.
[13] O. Shpotyuk, P. Baláž, Z. Bujňáková, A. Ingram, P. Demchenko, Ya. Shpotyuk, Mechanochemically-driven amorphization of nanostructurized arsenicals, the case of β-As_4S_4, J. Mater. Sci. 53 (2018) 13464–13476, https://doi.org/10.1007/s10853-018-2404-3.
[14] O. Shpotyuk, Z. Bujňáková, M.J. Sayagués, P. Baláž, A. Ingram, Ya. Shpotyuk, P. Demchenko, Microstructure characterization of multifunctional As_4S_4/Fe_3O_4 nanocomposites by complementary atomic-specific and atomic-deficient probes, Mater. Charact. 132 (2017) 303–311, https://doi.org/10.1016/j.matchar.2017.08.028.
[15] O. Shpotyuk, P. Demchenko, Y. Shpotyuk, Z. Bujňáková, P. Baláž, M. Hyla, V. Boyko, Amorphization diversity driven by high-energy mechanical milling in β-As4S4 polymorph, Mater. Today Commun. 21 (2019) 100679-1–100679-11, https://doi.org/10.1016/j.mtcomm.2019.100679.
[16] H. Heegn, Muhlen als Mechanoreaktoren, Chemie Ingenieur Technik 73 (2001) 1529–1539. https://doi.org/10.1002/1522-2640(200112)73:12<1529::AID-CITE1529>3.0.CO;2-N
[17] K. Tkacova, Mechanical Activation of Minerals, Elsevier, Amsterdam-Oxford-New York-Tokyo, 1989.
[18] N. Burgio, A. Iasonna, M. Magini, F. Padella, Mechanical alloying of the Fe-Zr system in different milling conditions, J. Phys. Colloques 51 (1990) C4-265-C4-271. 10.1051/jphyscol:1990432.
[19] J. Yang, X. Feng, G. Lu, Y. Li, C. Mao, Z. Wen, W. Yuan, NaCl as a solid solvent to assist the mechanochemical synthesis and post-synthesis of hierarchical porous MOFs with high I_2 vapour uptake, Dalton. Trans. 47 (2018) 5065–5071, https://doi.org/10.1039/c8dt00339d.
[20] E.J. Porter, G.M. Sheldrick, Crystal structure of a new crystalline modification of tetra-arsenic tetrasulphide (2,4,6,8-Tetrathia-1,3,5,7-tetra-arsatricyclo [3,3,0,$0^{3,7}$]-octane), J.C.S. Dalton 13 (1972) 1347–1349, https://doi.org/10.1039/DT9720001347.
[21] M.F. Fleet, The structure of magnetite, Acta Crystallogr. B 37 (1981) 917–920, https://doi.org/10.1107/S0567740881004597.

Please cite this article as: O. Shpotyuk, Z. L. Bujňáková, P. Baláž et al., Impact of grinding media on high-energy ball milling-driven amorphization in multiparticulate As_4S_4/ZnS/Fe_3O_4 nanocomposites, Advanced Powder Technology, https://doi.org/10.1016/j.apt.2020.07.008

[22] X. Fang, T. Zhai, U.K. Gautam, L. Li, L. Wu, Y. Bando, D. Golberg, ZnS nanostructures: From synthesis to applications, Progr. Meter. Sci. 56 (2011) 175–287, https://doi.org/10.1016/j.pmatsci.2010.10.001.
[23] J. Rodriguez-Carvajal, Recent developments of the program FullProf, Commission on Powder Diffraction (IUCr), Newsletter 26 (2001) 12–19.
[24] J. Rodriguez-Carvajal, T. Roisnel, Line broadening analysis using FullProf: determination of microstructural properties, Mater. Sci. Forum 443–444 (2004) 123–126, https://doi.org/10.4028/www.scientific.net/MSF.443-444.123.
[25] SRM 640b: silicon powder 2θ/d-spacing standard for X-ray diffraction, National Institute of Standards and Technology, U.S. Department of Commerce: Gaithersburg, MD, 1987.
[26] SRM 676: alumina internal standard for quantitative analysis by X-ray powder diffraction, National Institute of Standards and Technology, U.S. Department of Commerce: Gaithersburg, MD, 2005.
[27] S.C. Moss, D.L. Price, Random packing of structural units and the first sharp diffraction peak in glasses, in: D. Adler, H. Fritsche, S.R. Ovshinsky (Eds.), Physics of Disordered Materials, Plenum Publ. Corp., 1985, pp. 77–95. 10.1007/978-1-4613-2513-0_8.
[28] A. Zeidler, P.S. Salmon, Pressure-driven transformation of the ordering in amorphous network-forming materials, Phys Rev B 93 (2016) 214204-1–214204-5. 10.1103/PhysRevB.93.214204.
[29] P.S. Salmon, Real space manifestation of the first sharp diffraction peak in the structure factor of liquid and glassy materials, Proc. R. Soc. London A 445 (1994) 351–365, https://doi.org/10.1098/rspa.1994.0065.
[30] S.R. Elliott, Second sharp diffraction peak in the structure factor of binary covalent network glasses, Phys. Rev. B 51 (1995) 8599–8601, https://doi.org/10.1103/PhysRevB.51.8599.
[31] S.R. Elliott, Extended-range order, interstitial voids and the first sharp diffraction peak of network glasses, J. Non-Cryst. Solids 182 (1995) 40–48, https://doi.org/10.1016/0022-3093(94)00539-7.
[32] P.S. Salmon, R.A. Martin, P.E. Mason, G.J. Cuello, Topological versus chemical ordering in network glasses at intermediate and extended length scales, Nature 435 (2005) 75–78, https://doi.org/10.1038/nature03475.
[33] T. Roisnel, J. Rodriguez-Carvajal, WinPLOTR: a Windows tool for powder diffraction patterns analysis, Mater. Sci. Forum 118 (2001) 378–381. https://xray.chem.tamu.edu/pdf/manuals/winplotr_epdic.pdf.
[34] W. Kraus, G. Nolze, POWDER CELL – a program for the representation and manipulation of crystal structures and calculation of the resulting X-ray powder patterns, J. Appl. Cryst. 29 (1996) 301–303, https://doi.org/10.1107/S0021889895014920.
[35] J. Bletry, Sphere and distance models for binary disordered systems, Phil. Mag. B 62 (1990) 469–508, https://doi.org/10.1080/13642819008215248.
[36] Yu.I. Sozin, Diffractometry of coordination spheres, Crystallogr. Rep. 39 (1994) 6–13.
[37] O.P. Rachek, X-ray diffraction study of amorphous alloys Al-Ni-Ce-Sc with using Ehrenfest's formula, J. Non-Cryst. Solids 352 (2006) 3781–3786, https://doi.org/10.1016/j.jnoncrysol.2006.05.031.
[38] R. Feng, Z.H. Stachurski, M.D. Rodrigues, P. Kluth, L.L. Araujo, D. Bulla, M.C. Ridway, X-ray scattering from amorphous solids, J. Non-Cryst. Solids 383 (2013) 21–27, https://doi.org/10.1016/j.jnoncrysol.2013.04.070.
[39] P. Ehrenfest, On interference phenomena to be expected when Roentgen rays pass through a diatomic gas, In: KNAW, Proc. 17 (1914-1915) 1184-1190. https://www.dwc.knaw.nl/DL/publications/PU00012755.pdf.
[40] O. Shpotyuk, P. Demchenko, Y. Shpotyuk, Z. Bujňáková, P. Baláž, Medium-range structural changes in glassy As_2S_3 driven by high-energy mechanical milling, J. Non-Cryst. Solids 505 (2019) 347–353, https://doi.org/10.1016/j.jnoncrysol.2018.11.010.
[41] Ya. Shpotyuk, C. Boussard-Pledel, B. Bureau, P. Demchenko, J. Szlęzak, J. Cebulski, Z. Bujňáková, P. Baláž, O. Shpotyuk, Effect of high-energy mechanical milling on the FSDP-related XRPD correlations in Se-rich glassy arsenic selenides, J. Phys. Chem. Sol. 124 (2019) 318–326, https://doi.org/10.1016/j.jpcs.2018.09.036.
[42] Y. Shpotyuk, P. Demchenko, Z. Bujňáková, P. Baláž, C. Boussard-Pledel, B. Bureau, O. Shpotyuk, Effect of high-energy mechanical milling on the medium-range ordering in glassy As-Se, J. Am. Ceram. Soc. 103 (2020) 1631–1646, https://doi.org/10.1111/jace.16877.
[43] R. Bisaro, N. Proust, J. Magarino, Crystallization study of chemically vapour-deposited amorphous silicon films by in situ x-ray diffraction, Thin Solid Films 124 (1985) 171–177, https://doi.org/10.1016/0040-6090(85)90260-3.
[44] P. Baláž, M. Baláž, O. Shpotyuk, P. Demchenko, M. Vlcek, M. Shopska, J. Briancin, Z. Bujňáková, Y. Shpotyuk, L. Selepová, L. Balážová, Properties of arsenic sulphide (β-As_4S_4) modified by mechanical activation, J. Mater. Sci. 52 (2017) 1747–1758, https://doi.org/10.1007/s10853-016-0466-7.
[45] O. Shpotyuk, A. Kozdras, P. Balaz, Z. Bujnakova, Y. Shpotyuk, DSC TOPEM® study of high-energy mechanical milling-driven amorphization in β-As_4S_4-based arsenicals, J. Therm. Anal. Calorim. 135 (2019) 2935–2941, https://doi.org/10.1007/s10973-018-7613-0.
[46] O. Shpotyuk, S. Kozyukhin, Y. Shpotyuk, P. Demchenko, V. Mitsa, M. Veres, Coordination disordering in near-stoichiometric arsenic sulphide glass, J Non-Cryst Solids 402 (2014) 236–243, https://doi.org/10.1016/j.jnoncrysol.2014.06.013.
[47] O. Shpotyuk, A. Kozdras, P. Demchenko, Ya. Shpotyuk, Z. Bujňáková, P. Baláž, Solid-state amorphization of $As_{45}S_{55}$ alloy induced by high-energy mechanical milling, Thermochim. Acta 642 (2016) 59–66, https://doi.org/10.1016/j.tca.2016.09.009.
[48] M. Shpotyuk, O. Shpotyuk, V. Balitska, Combined configuration-enthalpy model describing radiation-optical responses in chalcogenide semiconductor glasses, Rad. Phys. Chem. 165 (2019) 108401-1–108401-5. 10.1016/j.radphyschem.2019.108401.
[49] John W. Anthony, Richard A. Bideaux, Kenneth W. Bladh, Monte C. Nichols, Eds., Handbook of Mineralogy, Mineralogical Society of America, Chantilly, VA 20151-1110, USA. http://www.handbookofmineralogy.org.
[50] P. Baláž, E. Boldižárová, E. Godočiková, J. Briančin, Mechanochemical route for sulphide nanoparticles preparation, Mater. Lett. 57 (2003) 1585–1589, https://doi.org/10.1016/S0167-577X(02)01037-6.
[51] Q.-Q. Zhao, G. Jimbo, The effect of grinding media on the breakage rate in a planetary ball mill, Adv. Powder Technol. 2 (1991) 91–101, https://doi.org/10.1016/S0921-8831(08)60709-8.
[52] R. Saravanan, S. Saravanakumar, S. Lavanya, Growth and local structure analysis of ZnS nanoparticles, Phys. B. 405 (2010) 3700–3703, https://doi.org/10.1016/j.physb.2010.05.069.
[53] Y.-W. Pan, S.-C. Qu, C.-X. Gao, Y.-H. Han, J.-F. Luo, Q.-L. Cui, J. Liu, G.-T. Zou, Structural phase transformations of ZnS nanocrystalline under high pressure, Chin. Phys. Lett. 21 (2004) 67–69, https://doi.org/10.1088/0256-307X/21/1/020.

Please cite this article as: O. Shpotyuk, Z. L. Bujňáková, P. Baláž et al., Impact of grinding media on high-energy ball milling-driven amorphization in multiparticulate As_4S_4/ZnS/Fe_3O_4 nanocomposites, Advanced Powder Technology, https://doi.org/10.1016/j.apt.2020.07.008